Characteristics of the boundary layer at Ny-Ålesund in the Arctic during the ARTIST field experiment

Stefania Argentini ([1])**, Angelo Pietro Viola** ([1])**, Giangiuseppe Mastrantonio** ([1])**, Alberto Maurizi** ([2])**, Teodoro Georgiadis** ([2]) **and Marianna Nardino** ([2])
([1]) *Istituto di Scienze dell'Atmosfera e del Clima (ISAC), CNR, Roma, Italy*
([2]) *Istituto di Biometeorologia (IBIMET), CNR, Bologna, Italy*

Abstract
A preliminary analysis of boundary layer data acquired during the Arctic Radiation and Turbulence Interaction Study Experiment (ARTIST) at Ny-Ålesund (Spitzbergen) in 1998 is presented. As expected, the wind field and the thermal structure of the boundary layer are strongly influenced by the katabatic flow blowing along the Kongsfjorden. In particular, if the large scale circulation has a component along the same direction, the resulting low level wind reaches velocities comparable with geostrophic wind. Stable to neutral conditions occurred most of the time, sustaining inversion or spiky layers respectively, depending on the wind intensity. The behaviour of some micrometeorological parameters was examined in relation to the general flow pattern and the characteristics of this area. The highest values of surface sensible heat flux (with negative sign) were observed during daytime, in presence of forced convection, due to the transfer of warmer upper layer air into the surface layer.

Key words *Arctic – planetary boundary layer – sodar – turbulence*

1. Introduction

A field experiment was carried out in Svalbard area in spring 1998 in the framework of the EC program ARTIST (Arctic Radiation and Turbulence Interaction Study). The objective of ARTIST was to improve the knowledge of the atmospheric properties during the sea-ice melting season and evaluate the relationship between the local dynamics, some micrometeorological parameters and the general flow pattern. The experiment was carried out by several European scientific institutions that provided airborne and ground-based measurements of wind, surface measurements of turbulence and radiation, as well as satellite and conventional meteorological data. A detailed description of the whole field programme, with the complete data inventory of ARTIST is given by Hartmann *et al.* (1999).

The present work highlights some observational results obtained from the analysis of ground-based and turbulent measurements at Ny-Ålesund in the Kongsfjorden in Spitzbergen Island. In particular, some aspects of the Arctic boundary layer structure, and the behaviour of the atmospheric parameters governing the boundary layer evolution are discussed in the general meteorological and geographical context.

2. Site and instrumentation

The Svalbard Islands are situated in the east part of the Arctic basin, 1000 km from the North Pole at an average latitude of 80°N.

The main island of Svalbard is Spitzbergen where the climatic influence of the Gulf Stream allows small communities to live there. The northernmost community lives in Ny-Ålesund (78.933°N, 11.933°E, 11 m a.s.l.) (fig. 1a,b) and principally cares about the Arctic station.

Due to the site characteristics and thanks to the logistic support of the Ny-Ålesund community, this place was chosen to carry out the turbulence and ground-based boundary layer measurements during the ARTIST field experiment that took place between March 15 and April 16, 1998.

The instrumentation employed in the field work included: a three-axis Doppler sodar, a tethersounding station, a micrometeorological station, a sensor to measure the ground flux, and three subsoil thermometers.

The sodar was located along the coast of the Kongsfjorden in the Zeppelin Bay (S in fig. 1b) to avoid the noise due to the human activity of the Ny-Ålesund village. The tethersounding station was set up along an old mine road at the foot of a small coal hill at about 20 m a.s.l. (T in fig. 1b) to avoid interference with the sodar measurements and to have free space to release the balloon. An ISO 20 container was also placed nearby to recover the balloon during strong wind episodes. The flight control and the data acquisition were done at the Italian Base (IB in fig. 1b). The mast with micrometeorological sensors was located between the sodar and the tethersounding station (R in fig. 1b).

The sodar, similar to the one used in some Antarctic campaigns by Argentini *et al.* (1992, 1996) is a monostatic three-axis Doppler system with 1.2 m diameter antennas that simultaneously emit three acoustic tones, one from each antenna, at 1750, 2000 and 2250 Hz. Two of the antennas were tilted 20° off the vertical, while the third one pointed vertically. The length of the acoustic pulse was 100 ms. The harmonic analysis of the signal to retrieve the radial wind was made with 0.16 s length samples, corresponding to approximately a 27 m depth layer, the first of which was at 50 m. The height reached by the sodar profiles ranged between 200 m and 900 m depending on the signal to noise ratio, and the wind conditions. A cross-beam configuration was chosen for the antennas; the tilted antennas were positioned at the acute vertices of a

rectangular triangle and oriented towards the vertically pointing antenna. As the vertical and tilted antennas were 25 m apart, they crossed at a height of 67 m. An angle of 30° was chosen between the Y axis and the North to avoid the noise from the Ny-Ålesund village.

The harmonic analysis of the received signal was then performed to derive the wind profile and to visualise the dynamic evolution of the airflow crossing the antenna's beam. The spectral analysis used to retrieve the Doppler shift and the echo intensity for each channel was carried out through a two-step procedure as explained by Mastrantonio and Fiocco (1982). For each channel, the processing of the returned signal provided the profiles of the radial wind velocity and echo intensity. The data were retained when a parameter related to the signal-to-noise ratio S/N exceeded the threshold of 0.75 (Mastrantonio and Fiocco, 1982).

The tethersounding system included a receiving ground station, and an airborne sensor package consisting of dry and wet bulb thermometers, pressure, wind speed and wind direction sensors and a 403.5 MHz transmitter. A 5 m^3 balloon, properly shaped to facilitate orientation upwind and retrievable by a winch with 1000 m of tetherline was used to fly the tethersonde. The temperature sensors have an accuracy of ± 0.5 °C. The wind speed, obtained by a three-cup anemometer, has an accuracy of ± 0.25 ms^{-1}, whereas the wind direction is measured with a magnetic compass that relies on the orientation of the balloon within an accuracy of ± 5°, when the balloon is suitably stable. An aneroid barometer measures the pressure with an accuracy of ± 1 hPa. During flight, the electronics of the tethersonde scanned the sensors sequentially and transmitted raw data to the ground station every 6 s. The altitude of the sensor package above the surface was estimated from the pressure and temperature profiles.

The balloon could be released only when the ground wind speed was less then 6 ms^{-1}. Before each launch a pre-flight control was conducted by measuring the temperature and pressure with ground sensors. The correct operation of the system (including battery check) and data quality were checked on-line to allow for any real time modification of the balloon flight.
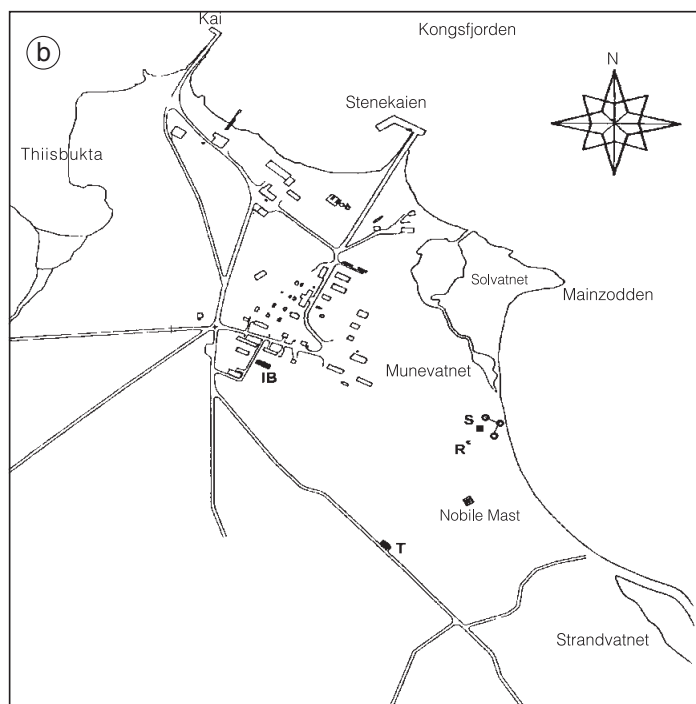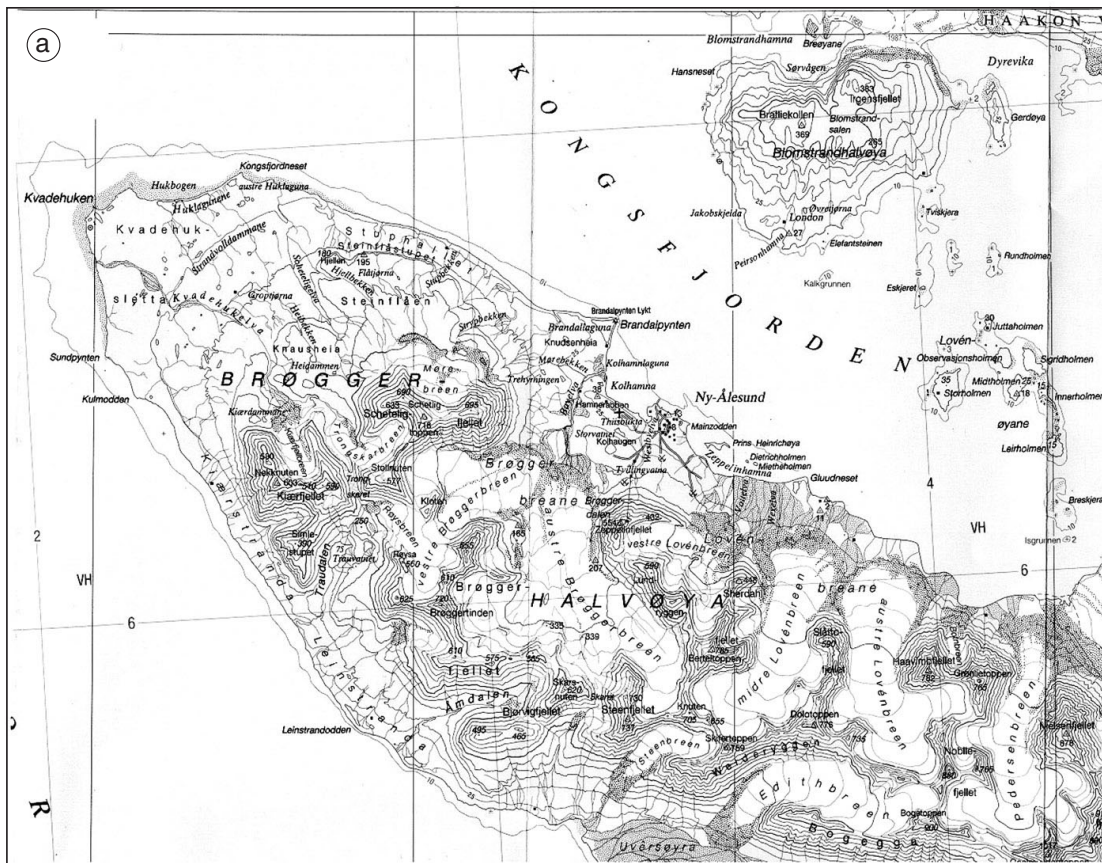
Fig. 1a,b. a) Map of the Kongsfjorden Spitsbergen Island; b) map of Ny-Ålesund and location of the experiment sites: 3-axes Doppler Sodar (S), Radiation and fast response sensors mast (R), Italian Base (IB), Tethersounding station (T).

The micrometeorological station was installed in a flat zone with little obstruction nearby. The instrumentation consisted of a Metek sonic thermo-anemometer (mod. USA-1) mounted on top of a 3 m mast, a fast response Campbell Kripton hygrometer (mod. KH20), and a Kipp and Zonen net radiometer (mod. CNR1).

The sonic thermo-anemometer was oriented to the north with an accuracy of 1.5°, and its vertical alignment was assured by two optical levels allowing a precision of 1°.

The fast hygrometer was used to estimate the latent heat flux by means of the eddy-covariance technique. Both sonic anemometer and fast hygrometer data were acquired at a frequency of 10 Hz and then collected by a MeteoFlux acquisition system (Sozzi and Favaron, 1996) to provide the real-time values of the three wind components and sonic temperature. Using three axis rotations (Sozzi and Favaron, 1996) the data were processed to derive all the turbulence variables, as well as, the sensible and the latent heat fluxes.

The net radiometer was used to determine the solar radiation budget. The incoming and outgoing components of the shortwave and longwave radiation were separately measured to derive the net radiation R_n. The shortwave net radiation S_{wn} was obtained by two pyranometers: one facing upward, to measure the incoming solar radiation and the other facing downward to measure the radiation reflected by the snow surface. The longwave net radiation L_{wn} was obtained by two pyrgeometers to measure the incoming and outgoing components separately. The self-heating of the instruments was controlled by a platinum-wire thermistor incorporated in the CNR1's body.

The sub-soil temperatures were measured using two termocouples buried in the snow at depths of 3 cm, 8 cm and 17.5 cm respectively.

3. Wind field observations

According to the climatology of the Spitzbergen (Førland *et al.*, 1997), the prevailing winds in the area blow from the NE-SE sector, except during the summer. However, the low-level circulation is strongly influenced by the orography and by flows of local origin. These flows, which move along valleys and fiords, are drainage winds transporting cold and heavy air from the inland glaciers to the warmer sea. These considerations refer to winds measured at 10 m by the weather stations located in the area. Since the sodar supplies vertical profiles, sometimes up to several hundred meters, it is possible to inspect whether the observed three-dimensional wind field is in agreement with the climatology and how it varies with height.

For about 12 days during the field experiment (from March 19 to April 1), the wind speed often reached peaks of 18 ms^{-1} with average values higher than seasonal observations. The noise created by high wind velocities caused strong limitations in the range of the sodar measurements.
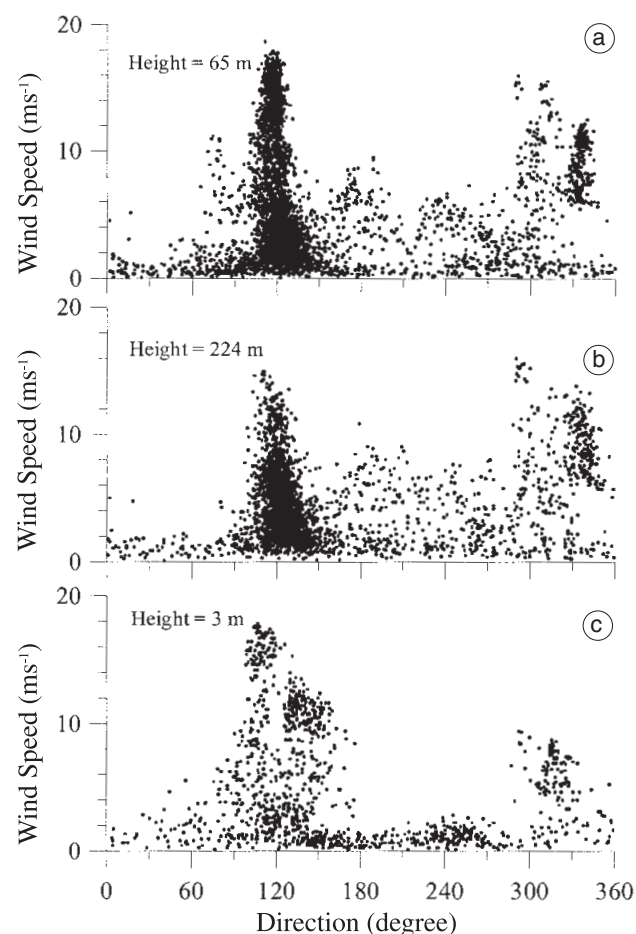
Fig. 2a-c. Scatter plot of the wind speed *versus* the wind direction during ARTIST at 65 m (a) and 224 m (b) for sodar and at 3 m for sonic data (c).

188
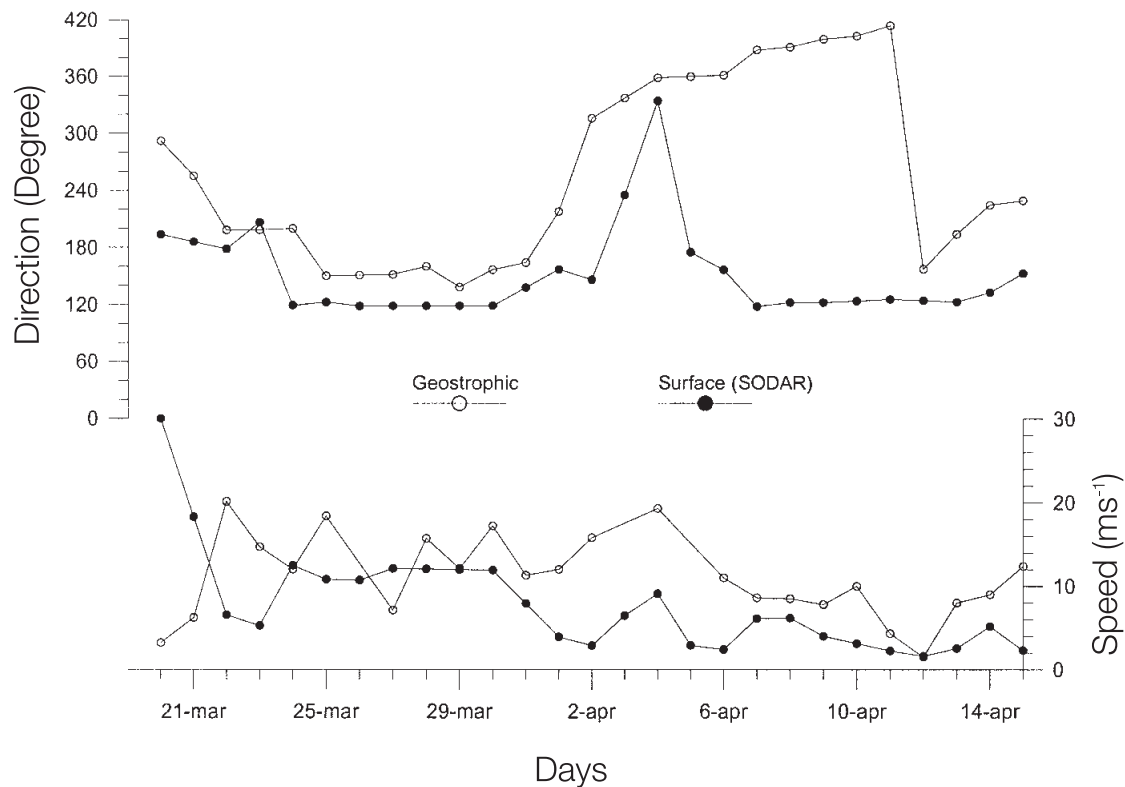
Fig. 3. Time series of the low level wind given by SODAR at 65 m, and the geostrophic wind by radiosounding during ARTIST at 1100 GMT.

Figure 2a-c reports the scatter plots of the wind speed against the wind direction at 65 m and 224 m (sodar), and 3 m (sonic anemometer), respectively. Above 224 m the statistics is too poor to yield an accurate description of the wind speed behaviour. As expected, the sonic anemometer data present a larger scatter due to the influence of local roughness.

Two main wind directions can be recognized: one around 100°-150°, along which the highest wind speeds are recorded, and one with a lower intensity peak at 300°-360°. These two directions correspond to the SE-NW geographic orientation of the Kongsfjorden, whose orographic characteristics are responsible for the forcing of the wind direction along this axis. The fact that the strongest winds are observed from SE sector mainly depends on synoptic circulation that often has a southern component. From the NW sector only flows with velocities greater than 6 ms^{-1} seem to overpass the mountains ridge north of the Kongsfjorden and reach Ny-Ålesund.
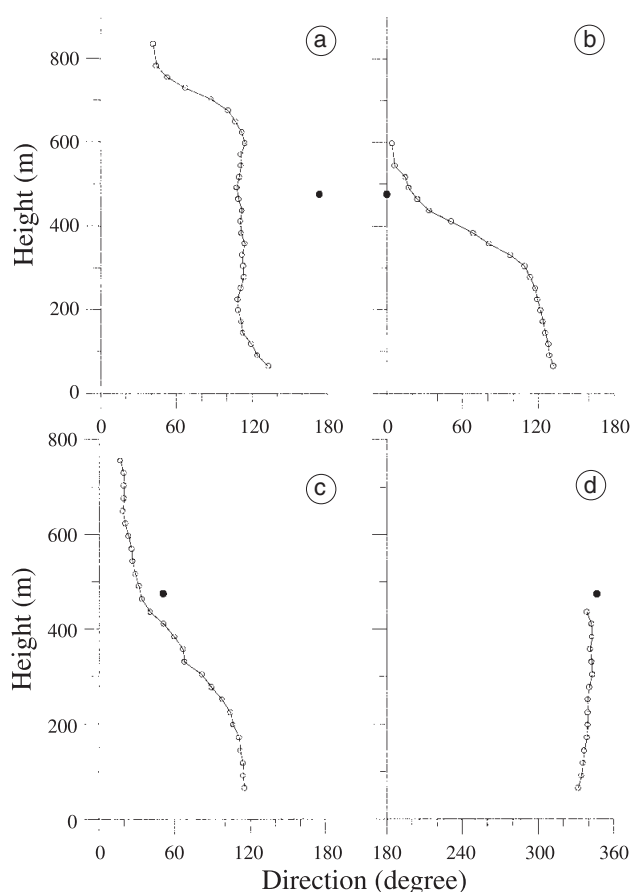
The wind dynamics in the fjord area of Ny-Ålesund is very complicated. Figure 2a-c shows that the wind speed at 65 m often exceeds that at 224 m. This is due to the existence of drainage flows, with a peak below 224 m, moreover a deviation of about 10°-20° from the mean direction for velocities higher than 8 ms^{-1} is evident at 65 m (fig. 2a) because the flow is less influenced by the local orography.

Figure 3 plots the direction and speed at 1100 GMT of the geostrophic and low level wind as a function of time. The geostrophic wind was obtained by using radiosoundings while the sodar data at 65 m were used for the low level wind. A difference of about 30°-40° is observed from March 24 to 30 when the wind speed at both level is about 10-14 ms^{-1}. In this case the geostrophic wind enhances the katabatic flow. Between April 6 and 12 the geostrophic wind rotates to the northern sector with a decline in the wind intensity although the low level wind still persist from E-SE. A large deviation (ranging

189

between 50° and 180°) is observed between the two flows. It would appear that in this case the geostrophic wind does not influence the flow along the Kongsfjorden which will be simply gravity driven downslope the glacier. This large rotation between the surface and geostrophic flows is determined by the position of the high-low pressure system, that causes a coupling of the low level and geostrophic circulation when the low pressure centre is located SW of Svalbard and a de-coupling when an opposite situation occurs.

An example of the three dominant flow patterns encountered at Ny-Ålesund is presented in fig. 4a-d. In order to show the role of the orography in this area, the wind direction measured at the research station on Mount Zeppelin at an altitude of 473 m (full dot) south
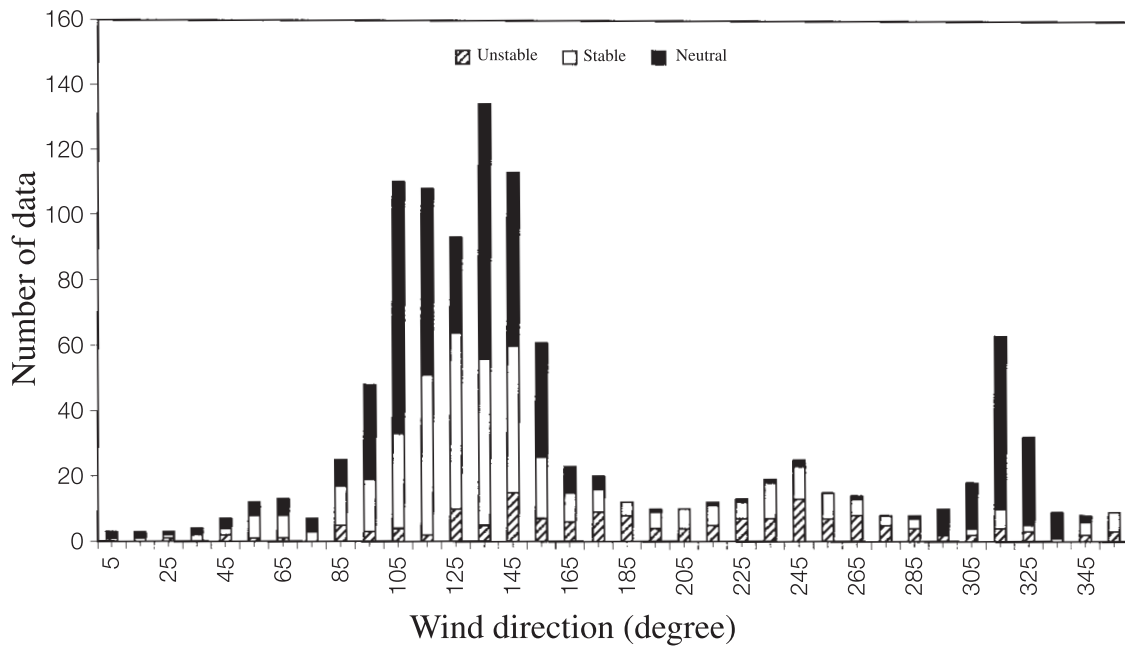
of Ny-Ålesund is also plotted. As shown by Beine *et al*. (2001), south-east flows are the most common situation at Ny-Ålesund. In fig. 4a a rotation of the wind direction is observed around 600 m. The depth of this layer is determined by the orographic influence on the large scale wind field and the presence of the katabatic wind in the lower level. Several superimposed flows may be present within this layer with the intensity of the katabatic flow determining the height of the katabatic layer. In other cases (fig. 4b,c) the katabatic flow was confined to the first 300-400 m while a superimposed flow blowing from 0-30° could be observed above 400 m. In both cases the sodar and the Zeppelin station observed, within a deviation of ± 10°, a northerly flow while the wind in Ny-Ålesund was from 120°. In the case of northerly flow at Ny-Ålesund, finally, the flow was from the same direction at the Zeppelin station (fig. 4d).

4. Thermal structure and stability of the atmosphere

The sonic anemometer data, even if they refer to point measurements, can provide quantities such as the Monin Obukhov length (L) which indicate the stability conditions of the boundary layer. The histogram in fig. 5 shows the statistics of z/L ($z = 3$ m is the height of the sensor) as a function of wind direction. These values were divided into three classes: according to unstable ($z/L < -0.05$), neutral ($-0.05 < z/L < 0.05$), and stable ($z/L > 0.05$) conditions. The plot shows two main peaks in the sectors centred around 120° and 310°, corresponding to the two predominant wind directions. Most of the time neutral conditions occur in these two sectors. Stable conditions with thermal stratifications at different levels are mainly observed when the wind blows in the sector centred at 120°. Unstable situations, occurring under very light wind conditions, can span from 90° to 270°, with a peak at 245°. The predominant structures observed by the sodar during the experiment were spiky layer, caused by forced convection, in the first period of the campaign until April 1 and stable stratifications, often modulated by internal gravity waves, generated by shear of the

Fig. 4a-d. Typical 1 h averaged wind profiles (circle) observed at Ny-Ålesund, the wind direction measured at the Zeppelin research station (full dot) is given for comparison. a) April 7 between 2000-2100 ST; b) April 6 between 0900-1000; c) April 5 between 1900-2000; d) April 5 between 0200-0300.

Fig. 5. Histogram with the distribution of the observed cases for three different stability classes, unstable: $z/L < -0.05$; neutral: $-0.05 < z/L < 0.05$; stable: $z/L > 0.05$ during ARTIST.

basic flow. These features generally alternated depending on the wind intensity, cloud cover, sunshine factor and large scale flow.

Forced convection occurred because of the presence of a large wind shear in the first 100-300 m generating anisotropic turbulence primarily in the horizontal direction. The resulting spiky structures are similar to those observed in Antarctica by Gera *et al.* (1998). Figure 6a shows an example of these structures on March 26. The wind had velocities up to 15 ms⁻¹, and the direction was mainly from 120°. Unfortunately, the noise generated by the wind did not allow us to derive the profiles above 300-400 m. Large instantaneous values of the vertical velocity of the order of 2 ms⁻¹ (not shown in this paper) were also associated with these high wind velocities. The vertical mixing due to the forced convection produced an almost neutral layer with the stability parameter *z/L* very close to zero as shown in fig. 6b. This process was responsible for the neutral or lightly stable cases presented in fig. 5.

Stable stratifications were observed when the wind velocity was lower than 5-6 ms⁻¹. In these conditions, the sodar measurements could range up to 1000 m. An example of the observed stratifications as well as the horizontal wind

profiles are shown in fig. 7a,b for April 7. Three inversion layers topped by a zone of enhanced thermal stability and relevant wind shear at about 150 m, 400 m and 700 m are present together with Kelvin-Helmotz waves of different frequency. The horizontal wind shear increases at thermal turbulent layer height (fig. 7a) as was also observed by Overland (1985) and Curry *et al.* (1988). During a field experiment in the Fram Strait north-west of the Svalbard, Brummer *et al.* (1994) also observed four sublayers below 1700 m topped by moisture inversions (zones of enhanced moisture). Busak and Brummer (1988), using vertical soundings from one flight mission over the North Sea, also showed that despite the stable temperature stratifications, the wind shear at certain levels is sufficiently large for the Richardson number to be below its critical value of 0.25 and coherent motions – in the form of Kelvin Helmoltz waves – may be generated under these conditions. The presence of the Kelvin-Helmholtz waves makes the determination of the inversion height difficult because of the strong oscillations.

The stability parameter *z/L* calculated for April 7 (fig. 7b), oscillates between positive and negative values. Although the waves develop in
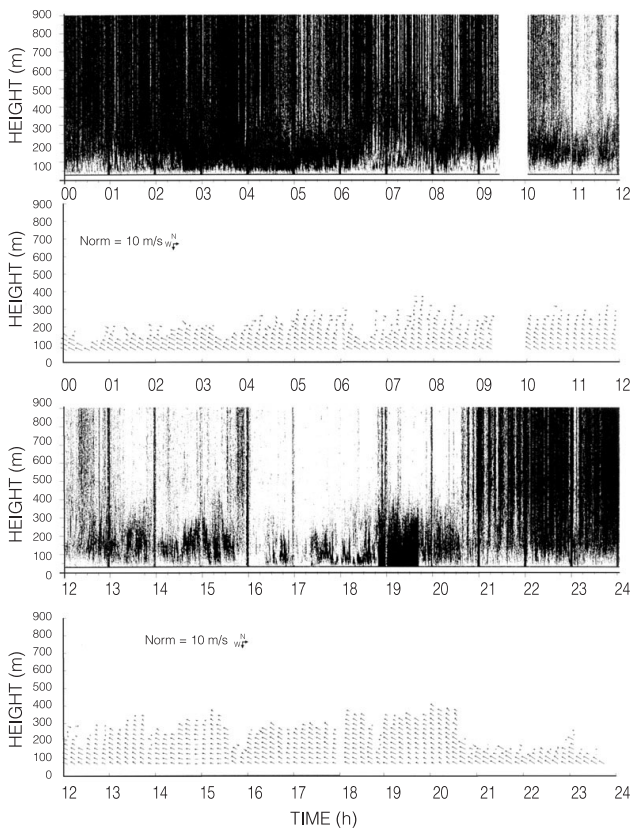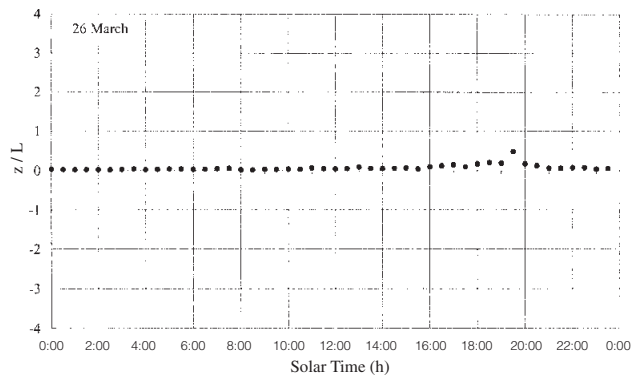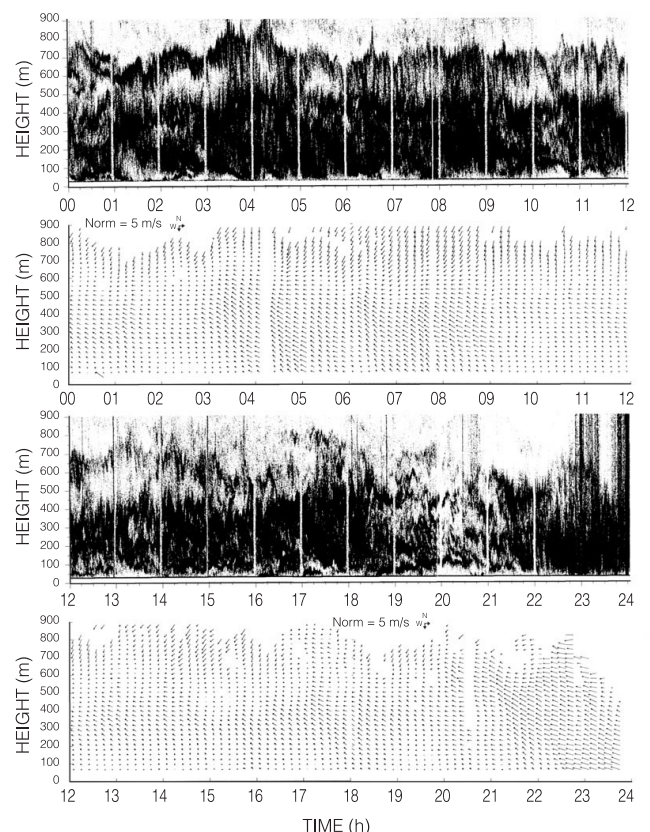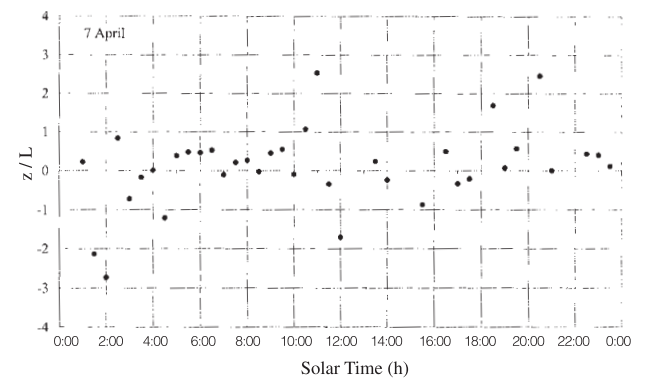
Fig. 6a,b. a) Sodar facsimile and horizontal velocity recorded at Ny-Ålesund on March 26, 1998 during forced convection; b) stability parameter *z/L* as a function of solar time.

Fig. 7a,b. a) Sodar facsimile and horizontal velocity recorded at Ny-Ålesund on April 7, 1998 showing a stable layer with waves; b) stability parameter *z/L* as a function of solar time.

a stable boundary layer, these oscillations may be attributed to upward and downward oscillations of air masses with different thermal and dynamic characteristics. Although these values are not representative of the «real» stability conditions, they are sufficiently indicative of the thermal structure of the atmosphere to be used as an indicator of the presence of waves.

192

Use of the sodar for measuring the turbulent components of the wind is still problematic (Wilczak *et al.*, 1996), but some quantities such as the variance of the vertical velocity give values that are correct if the data are properly analysed. In these cases, as shown by Angevine *et al.* (1994) and Argentini *et al.* (1999), these values are more representative than *in situ* surface measurements, since they are less sensitive to surface conditions than a point sensor.

5. Surface fluxes

The surface fluxes have been calculated from the covariances of the temperature, humidity and vertical fluctuations, using sonic anemometer and fast hygrometer measurements.

The behaviour of the sensible heat flux (H_0), Turbulent Kinetic Energy (TKE), and of vertical momentum fluxes ($u'w'$), for the whole measurement period are presented in fig. 8 a,b
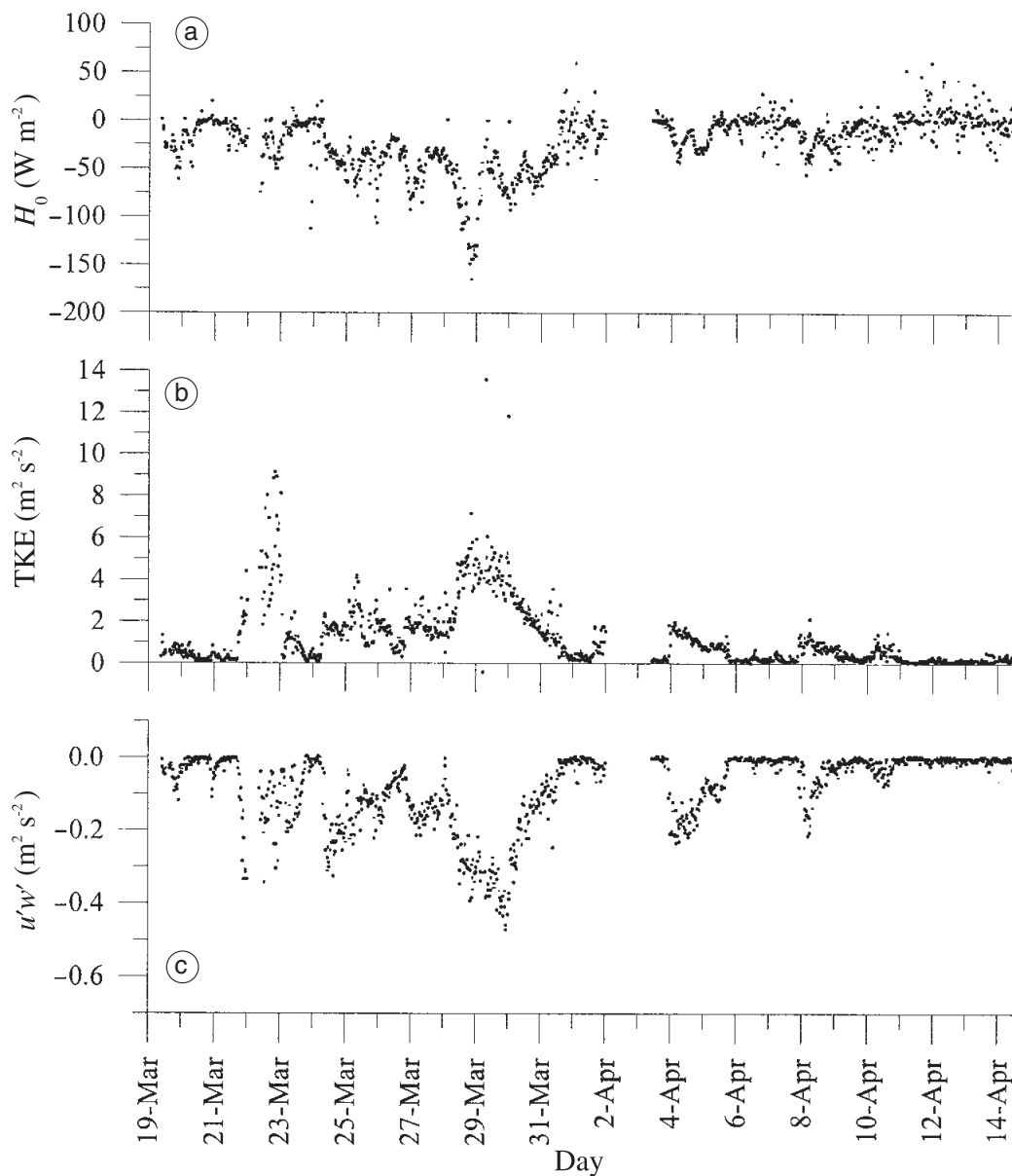
Fig. 8a-c. a) Behaviour of the sensible heat flux; b) turbulent kinetic energy; c) vertical momentum flux, during ARTIST.

and c, respectively. Until the end of March the sensible heat flux is, most of the time, negative as expected under stable atmospheric conditions. The highest values of sensible heat flux, TKE and momentum flux are reached for strong wind speeds. When the mechanical turbulence is high, the strong vertical mixing produces a remarkable sensible heat flux transfer from the atmosphere to the surface (negative sign). During the last measurement period (early to mid-April), characterised by weaker winds and a low cloud coverage (as pointed out later), the sensible heat flux tends to assume positive values (convective atmospheric conditions).

It is noted that the behavior of TKE and momentum flux are negatively correlated. The radiative budget at the surface, obtained through the radiometric measurements, is shown in fig. 9. The low values of the net radiation R_n indicate that very low energy is available at these latitudes. The shortwave net flux S_{wn} has an increasing trend due to the increase in the daytime period. The
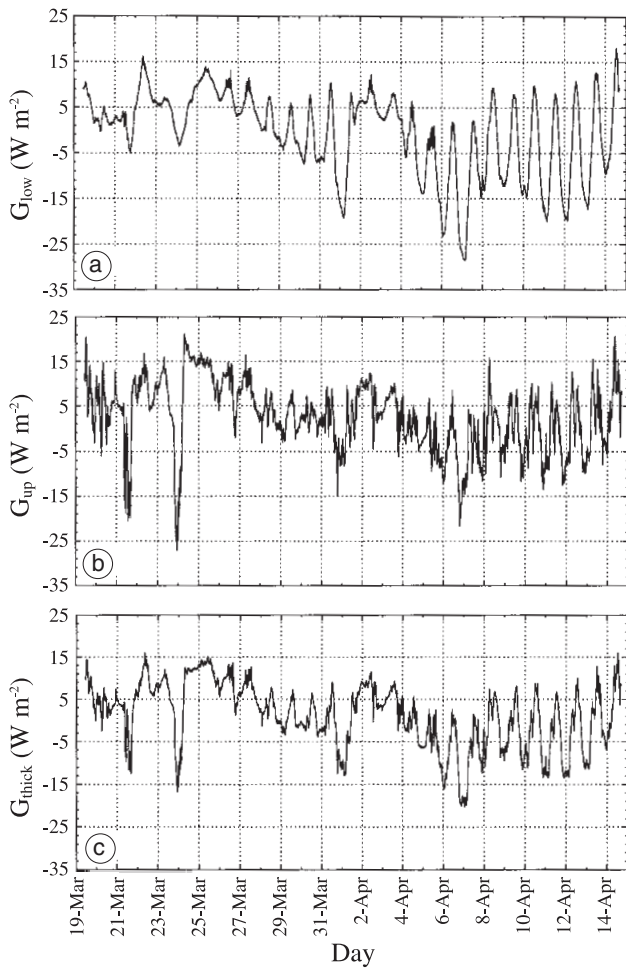
straight lines in the S_{wn} and R_n plots are due to the shadow of the mast on the radiometer. The first measurement period was characterised by intense cloud coverage days with very low values of S_{wn} and irregular behaviour. Low cloud coverage was present after April 4.

Finally, the value of the sub-surface flux through the measurements of the snow temperature at different depth was calculated.

The value of the flux in the soil, if no water-phase changes occur at the surface, is given by two terms: one due to the heat transferred by conduction and the other caused by transmission of the shortwave radiation into the snow (Bintanja and van den Broeke, 1995). This parameterisation was applied to our measurements using two snow temperatures to obtain the conduction heat, and the shortwave radiation component for the radiative heating. Figure 10 a-c shows the values of the fluxes into the snow obtained using three different temperature gradients; G_{low} using the difference between T_2 and T_3, G_{up}
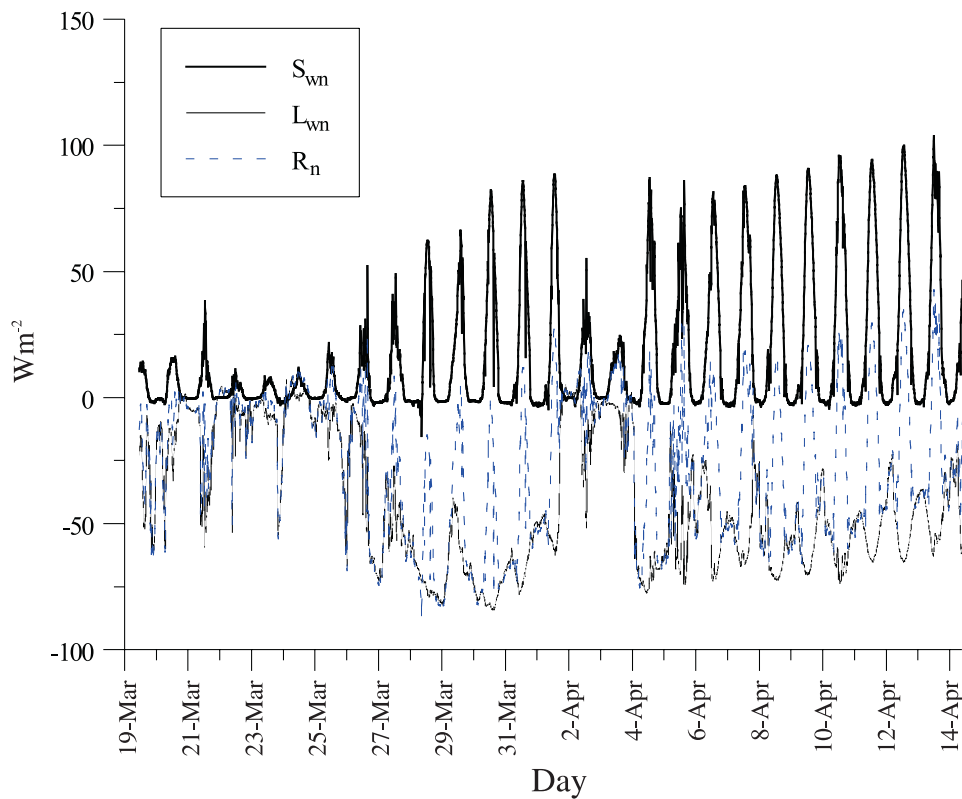
Fig. 9. Behaviour of the net radiation, longwave net radiation and shortwave net radiation for the whole measurement period.

194

Fig. 10a-c. Time evolution of the flux into the snow calculated with three different temperature gradients: a) $T_2 - T_3$ for G_{low}; b) $T_1 - T_2$ for G_{up}, and c) $T_1 - T_3$ for G_{thick}, being T_1 at 3 cm, T_2 at 8 cm and T_3 at 17.5 cm below the surface respectively.

the measurement campaign show a higher value of the flux into the snow. Moreover, during night time in clear days the G_{low} values were almost 10 Wm^{-2} lower than the corresponding G_{up} values. This can be explained considering that during the night the surface temperature and the snow temperature at 8 cm decreased following almost the same slope, whereas the snow temperature at 17.5 cm decreased more gently, so that the difference between the decreasing rate of T_2 and T_3 was larger than between T_1 and T_2. These temperature differences indicate that the sensor T_2 is not deep enough to account for all heat stored in the snow or released toward the surface during the day. The sensor T_3 is probably at the most appropriate reference depth for calculating heat exchanges between the surface and the deepest layers.

6. Summary

We have presented some preliminary observational results from the ground-based measurements during the field experiment ARTIST in Ny-Ålesund. Neutral conditions were observed from the two predominant wind directions centred in the 120° and 310° sectors. A minor peak with the 20% of unstable cases was observed at 245° while stable conditions were mainly distributed around the sector at 120°. The thermal structure of the atmosphere was recorded with a sodar system. Two main features were observed: spiky layers and stable stratifications. Spiky layers, due to the presence of forced convection, were observed in correspondence of high wind speed, stratified flows with waves occurred for low wind velocities. The two features mostly alternated with each other depending on the wind intensity. To further characterise wavy and well mixed layers, the vertical velocity variances were measured over time, using the sonic anemometer and the sodar. A general consistency was observed between the two sets of data during forced convection when the atmosphere, under the influence of strong mechanical mixing along the vertical, presents air masses with similar properties at the two sensors. A comparison between the wind in the boundary layer and the geostrophic wind estimated by radiosoundings

between T_1 and T_2 and, G_{thick} between T_1 and T_3. The general behaviour of G_{low} is smoother than the corresponding G_{up} and G_{thick} calculated in the uppermost and thickest layers respectively. This is a direct consequence of the smaller fluctuations at greater depths. Ground fluxes minima are observed when the surface temperature reaches a minimum (generally during the night). Under these conditions the snow temperature in the deeper layers is higher than at the surface and the heat flux is directed upwards.

In interpreting these results we should bear in mind that G_{up} is surely over-estimated because the upper part of the temperature sensor tends to heat itself during clear days. Indeed, the last days of

was undertaken. For moderate to high wind speed a deviation of about 30° is observed between the two directions; in this case the geostrophic wind contributes to enhance the katabatic flow intensity and persistence. A deviation (ranging between 50° and 180°) was observed for weak winds.

The highest values of the sensible heat fluxes were observed during day time under forced convection because of the transfer of warmer upper layer air into the surface layer.

The radiometric and temperature measurements were utilised to compute the net radiation and subsurface heat flux. The flux into the snow depends on several factors such as the depth of the snow layer, the thermal conductivity and the fraction of solar radiation absorbed by the surface. An analysis of gradient fluxes G, obtained for different snow layers, showed that the most representative values are those of the layer between the surface and the deepest temperature sensor. However, further studies are necessary to arrive at more complete parameterisation schemes of the conductive and radiative components of the subsurface heat flux.

Acknowledgements

REFERENCES

ANGEVINE, W.M., R.J. DOVIAK and Z. SORBJAN (1994): Remote sensing of vertical velocity variance and surface heat flux in a convective boundary layer, *J. Appl. Meteorol.*, **33** (8), 977-983.

ARGENTINI, S., G. MASTRANTONIO, G. FIOCCO and R. OCONE (1992): Complexity of the wind field as observed by a sodar system and by automatic weather stations on the Nansen Ice Sheet, Antarctica, during summer 1988-1989: two cases studies, *Tellus*, **44B**, 422-429.

ARGENTINI, S., G. MASTRANTONIO, A. VIOLA, P. PETTRÉ and G. DARGAUD (1996): Sodar performances and preliminary results after one year measurements at Adelie coast, East Antarctica, *Boundary Layer Meteorol.*, **81**, 75-103.

ARGENTINI, S., G. MASTRANTONIO and F. LENA (1999): The convective boundary layer during winter in the urban aerea of Milano: a few cases study, *Boundary Layer Meteorol.*, **93**, 253-267.

BEINE, H.J., S. ARGENTINI, A. MAURIZI, G. MASTRANTONIO and A. VIOLA (2001): The local wind field a Ny-Ålesund and Zeppelin mountain at Svalbard, *Meteorol. Atmos. Phys.*, **78**, 107-113.

BINTANJA, R. and M.R. VAN DEN BROEKE (1995): The surface energy balance of Antarctic snow Blue Ice, *J. Appl. Meteorol.*, **34**, 902-926.

BRUMMER, B., B. BUSAK, H. HOEBER and G. KRUSPE (1994): Boundary-layer observations over water and Arctic sea-ice during on-ice air flow, *Boundary Layer Meteorol.*, **68**, 75-108.

BUSAK, B. and B. BRUMMER (1988): A case study of Kelvin-Helmholtz waves within an off-shore stable boundary layer: observations and linear model, *Boundary Layer Meteorol.*, **44**, 105-135.

CURRY, J.A., E.E. EBERT and G.F. HERMAN (1988): Mean and turbulence structure of the summertime Arctic cloudy boundary layer, *Q. J. R. Meteorol. Soc.*, **114**, 715-746.

FØRLAND, E.J., I. HANSEN-BAUER and P.Ø. NORDLI (1997): Climate statistics and long-term series of temperature and precipitation at Svalbard and Jan Mayen, Den Norske Meteorologiske Institutt, Oslo, Norway, *Rep. OMNI 39/90 KLIMA*, pp. 40.

GERA, B.S., S. ARGENTINI, G. MASTRANTONIO, A. VIOLA and A. WEILL (1998): Characteristics of the boundary layer thermal structure at a coastal region of Adelie land, East Antarctica, *Antarct. Sci.*, **10** (1), 89-98.

HARTMANN, J., F. ALBERS, S. ARGENTINI, A. BOCHERT, U. BONAFÈ, W. COHRS, A. CONIDI, D. FREESE, T. GEORGIADIS, A. IPPOLITI, L. KALESCHKE, C. LUPKES, U. MAIXNER, G. MASTRANTONIO, F. RAVEGNANI, A. REUTER, G. TRIVELLONE and A. VIOLA (1999): Arctic Radiation and Turbulence Interaction Study (ARTIST), Alfred-Wegener-Institute für Polar Meeresforschung, Bremerhaven, Germany, *Rep. on Polar Research 305/1999*, pp. 81.

MASTRANTONIO, G. and G. FIOCCO (1982): Accuracy of wind velocity determination with doppler sodar, *J. Appl. Meteorol.*, **21**, 820-830.

OVERLAND, J.E. (1985): Atmospheric boundary layer structure and drag coefficients over sea ice, *J. Geophys. Res.*, **90** (5), 9029-9049.

SOZZI, R. and M. FAVARON (1996): Sonic anemometry and thermometry: theoretical basis and data-processing software, *Environ. Software*, **11** (4), 259-270.

WILCZAK, J.M., E.E. GOSSARD, W.D. NEFF and L. EBERHARD (1996): Ground-based remote sensing of the atmospheric boundary layer: 25 years of progress, *Boundary Layer Meteorol.*, **78**, 321-349.